



Published as: *Cell*. 2008 October 17; 135(2): 295–307.

## THE RNA POLYMERASE “SWITCH REGION” IS A TARGET FOR INHIBITORS

Jayanta Mukhopadhyay<sup>1,2,4,\*</sup>, Kalyan Das<sup>3,4,\*</sup>, Sajida Ismail<sup>1,2,4</sup>, David Koppstein<sup>1,2,4</sup>,  
Minyoung Jang<sup>1,2,4</sup>, Brian Hudson<sup>3,4</sup>, Stefan Sarafianos<sup>3,4</sup>, Steven Tuske<sup>3,4</sup>, Jay Patel<sup>3,4</sup>,  
Rolf Jansen<sup>5</sup>, Herbert Irschik<sup>5</sup>, Eddy Arnold<sup>3,4,\*\*</sup>, and Richard H. Ebright<sup>1,2,4,\*\*</sup>

<sup>1</sup> Howard Hughes Medical Institute, Rutgers University, Piscataway NJ 08854

<sup>2</sup> Waksman Institute, Rutgers University, Piscataway NJ 08854

<sup>3</sup> Center for Advanced Biotechnology and Medicine, Rutgers University, Piscataway NJ 08854

<sup>4</sup> Department of Chemistry and Chemical Biology, Rutgers University, Piscataway NJ 08854

<sup>5</sup> Helmholtz Centre for Infection Research, Braunschweig, Germany

### Summary

We report the target, biochemical basis, and structural basis of inhibition of bacterial RNA polymerase (RNAP) by the  $\alpha$ -pyrone antibiotic myxopyronin (Myx). We show that Myx interacts with the RNAP “switch region,” the hinge that mediates opening and closing of the RNAP active-center cleft. We show that Myx prevents interaction of RNAP with promoter DNA. We present a crystal structure that defines contacts between Myx and RNAP and defines effects of Myx on RNAP conformation. We propose that Myx functions by preventing opening of the RNAP active-center cleft to permit entry of DNA during transcription initiation (“hinge jamming”). We establish further that the structurally related  $\alpha$ -pyrone antibiotic coralopyronin and the structurally unrelated macrocyclic-lactone antibiotic ripostatin function through the same target and same mechanism. The RNAP switch region is an attractive target for identification of new broad-spectrum antibacterial therapeutic agents.

### Introduction

Bacterial RNA polymerase (RNAP) is a proven target for broad-spectrum antibacterial therapy (Darst et al., 2004; Chopra, 2007). The suitability of bacterial RNAP as a target for broad-spectrum antibacterial therapy follows from the fact that bacterial RNAP is an essential enzyme (permitting efficacy), the fact that bacterial RNAP subunit sequences are highly conserved (permitting for broad-spectrum activity), and the fact that bacterial RNAP-subunit sequences and eukaryotic RNAP-subunit sequences are not highly conserved (permitting therapeutic selectivity).

\*\*To whom correspondence should be addressed: ebright@mbcl.rutgers.edu, arnold@cabm.rutgers.edu.

\*Contributed equally

Corresponding Author: Richard H. Ebright, Address: Waksman Institute, Rutgers University, Piscataway NJ 08854, USA, Telephone: (732) 445-5179, Telefax: (732) 445-5735, Email: ebright@mbcl.rutgers.edu

**Publisher's Disclaimer:** This is a PDF file of an unedited manuscript that has been accepted for publication. As a service to our customers we are providing this early version of the manuscript. The manuscript will undergo copyediting, typesetting, and review of the resulting proof before it is published in its final citable form. Please note that during the production process errors may be discovered which could affect the content, and all legal disclaimers that apply to the journal pertain.

The rifamycin antibacterial agents--notably rifampicin, rifapentine, and rifabutin--function by binding to and inhibiting bacterial RNAP (Campbell et al., 2001; Darst et al., 2004; Chopra, 2007). The rifamycins bind to a site on bacterial RNAP adjacent to the RNAP active center and prevent extension of RNA beyond a length of 2–3 nt. The rifamycins are of clinical importance in treatment of Gram-positive and Gram-negative bacterial infections, are first-line antituberculosis agents, and are the only antituberculosis agents able rapidly to clear infection and prevent relapse. However, the clinical utility of the rifamycin antibacterial agents is threatened by the existence of bacterial strains resistant to rifamycins. Resistance to rifamycins typically involves substitution of residues in or adjacent to the rifamycin binding site on bacterial RNAP--i.e., substitutions that directly decrease binding of rifamycins.

In view of the public-health threat posed by rifamycin-resistant and multidrug-resistant bacterial infections, there is an urgent need for new classes of antibacterial agents that (i) target bacterial RNAP (and thus have the same biochemical effects as rifamycins), but that (ii) target sites within bacterial RNAP distinct from the rifamycin binding site (and thus do not show cross-resistance with rifamycins) (Darst et al., 2004; Chopra, 2007).

Structures have been determined for bacterial RNAP and eukaryotic RNAP II (Zhang et al., 1999; Cramer et al., 2000,2001; Ebright, 2000; Darst, 2001; Cramer, 2002; Young et al., 2002; Murakami and Darst, 2003). The structures reveal that RNAP--bacterial or eukaryotic--has dimensions of  $\sim 150 \text{ \AA} \times \sim 100 \text{ \AA} \times \sim 100 \text{ \AA}$  and has a shape reminiscent of a crab claw (Fig. 1A). The two “pincers” of the “claw” define the active-center cleft, which has a diameter of  $\sim 20 \text{ \AA}$ --a diameter that can accommodate a double-stranded nucleic acid--and which has the active-center  $\text{Mg}^{2+}$  at its base. The largest subunit ( $\beta'$  in bacterial RNAP) makes up one pincer, termed the “clamp,” and part of the base of the active-center cleft. The second-largest subunit ( $\beta$  in bacterial RNAP) makes up the other pincer and part of the base of the active-center cleft.

The structures further reveal that the RNAP clamp can exist in a range of distinct conformational states--from a fully open clamp conformation that permits unimpeded entry and exit of DNA (clamp perpendicular to floor of active-center cleft), to a fully closed clamp conformation that prevents entry and exit of DNA (clamp rotated into active-center cleft) (Fig. 1A; Zhang et al., 1999; Cramer et al., 2000,2001; Ebright, 2000; Darst, 2001; Cramer, 2002; Young et al., 2002; Murakami and Darst, 2003). The transition between the fully open and fully closed clamp conformations involves a  $30^\circ$  swinging motion of the clamp, with a  $30 \text{ \AA}$  displacement of residues at the distal tip of the clamp (Fig. 1A). It has been proposed that the clamp must open to permit DNA to enter the active-center cleft during early stages of transcription initiation, and that the clamp must close to retain DNA in the active-center cleft during later stages of transcription initiation and during transcription elongation.

The “switch region” is located at the base of the clamp and serves as the hinge on which the clamp swings in clamp opening and clamp closure (Fig. 1B; Cramer et al., 2001; Gnatt et al., 2001; Cramer, 2002). The switch region adopts different conformations in open and closed clamp conformational states (Fig. 1B). Several residues of the switch region make direct contacts with DNA phosphates in the transcription elongation complex (Gnatt et al., 2001; Vassilyev et al., 2007). It has been proposed that direct contacts between the switch region and DNA phosphates might coordinate, and even might mechanically couple, clamp closure and DNA binding (Cramer et al., 2001; Gnatt et al., 2001; Cramer, 2002).

In this work, we show that three antibiotics--the  $\alpha$ -pyrone antibiotic myxopyronin (Myx), the  $\alpha$ -pyrone antibiotic coralopyronin (Cor), and the macrocyclic-lactone antibiotic ripostatin (Rip)--function by binding to the RNAP switch region and preventing interaction of RNAP with promoter DNA, apparently by preventing opening of the clamp to permit entry of promoter DNA during transcription initiation. The three compounds interact with residues that are

conserved in Gram-positive and Gram-negative bacterial RNAP, and, accordingly, exhibit broad-spectrum antibacterial activity. The three compounds interact, in part, with residues that are not conserved in eukaryotic RNAP I, RNAP II, and RNAP III, and, accordingly, do not exhibit cross-inhibition of eukaryotic RNAP. The three compounds interact with residues that are remote from the binding site for rifamycins and from the binding sites for other characterized RNAP inhibitors (Fig. 1A), and, accordingly, do not exhibit cross-resistance with rifamycins or other characterized RNAP inhibitors (Table 1). Taken together, these properties make the three compounds attractive candidates for development as broad-spectrum antibacterial therapeutic agents and make the switch region an attractive target for identification of new broad-spectrum antibacterial therapeutic agents.

## Results

### Target of transcription inhibition by Myx

**Myx**—Myx is polyketide-derived  $\alpha$ -pyrone antibiotic produced by the myxobacterium *Myxococcus fulvus* Mxf50 (Fig. 1C; Irschik et al., 1983; Kohl et al., 1983). The compound inhibits growth of a broad spectrum of Gram-positive and Gram-negative bacterial species, including *Mycobacterium tuberculosis*, *Staphylococcus aureus*, *Bacillus anthracis*, *Enterococcus faecium*, *Enterobacter cloacae*, *Acinetobacter calcoaceticus*, *Pseudomonas aeruginosa*, and *Escherichia coli* DH21toIC (MICs  $\leq 12.5$   $\mu\text{g/ml}$  for all; MICs  $\leq 1$   $\mu\text{g/ml}$  for *S. aureus*, *A. calcoaceticus*, and *E. coli* DH21toIC; Irschik et al., 1983; Kohl et al., 1983; Hu et al., 1998; M. Talaue, N. Connell, J.M., and R.H.E. unpublished). The compound is bacteriocidal, as assessed with *E. coli* DH21f2toIC (J.M. and R.H.E. unpublished). The compound inhibits bacterial RNAP (IC<sub>50</sub>  $\sim 1$   $\mu\text{M}$ ) but does not inhibit eukaryotic RNAP II (Irschik et al., 1983). The compound exhibits no acute toxicity in mice at concentrations up to 100 mg/kg (Irschik et al., 1983). Total syntheses of Myx have been reported, and analogs of Myx have been prepared (Hu et al., 1998; Doundoulakis et al., 2004; Lira et al., 2007). However, in the absence of information regarding the target, biochemical basis, and structural basis of transcription inhibition by Myx, efforts to prepare more potent analogs have been unsuccessful.

**The RNAP switch region contains a determinant for function of Myx**—As a first step to identify the target within RNAP for Myx, we performed random mutagenesis of the genes encoding *E. coli* RNAP  $\beta'$  and  $\beta$  subunits, and isolated and characterized mutants conferring resistance to Myx (Myx<sup>r</sup>). We identified four different single-substitution Myx<sup>r</sup> mutants: two involving substitution of residue 345 within conserved region C of  $\beta'$  subunit, and one each involving substitution of residues 1275 and 1291 within conserved region I of  $\beta$  subunit (Table S1; Fig. S1A).

Minimum-inhibitory-concentration (MIC) assays indicate that all four Myx<sup>r</sup> mutants exhibit  $\geq 2$ -fold increases in MIC, and that three of four Myx<sup>r</sup> mutants exhibit  $\geq 32$ -fold increases in MIC (Table S1). Complementation assays indicate that each Myx<sup>r</sup> mutant is able to complement a corresponding temperature-sensitive mutant for growth at the non-permissive temperature, indicating that each Myx<sup>r</sup> RNAP derivative is functional in transcription--sufficiently functional to support viability (Table S1). In the three-dimensional structure of RNAP, the sites of the Myx<sup>r</sup> substitutions cluster tightly and are located in the RNAP switch region (Fig. 2A). We conclude that the RNAP switch region contains a determinant required for transcription inhibition by Myx.

**The RNAP switch region contains an extensive determinant for function of Myx**—To define systematically the determinant for Myx within the RNAP switch region, we performed saturation mutagenesis of the genes encoding the RNAP  $\beta'$  and  $\beta$  subunits, and isolated and characterized additional Myx<sup>r</sup> mutants. We performed saturation mutagenesis

using a set of seventeen “doped” oligonucleotide primers designed to introduce all possible nucleotide substitutions at all codons for all residues located within 30 Å of the Myx<sup>r</sup> substitutions of the preceding paragraph (sequences in Table S2). We isolated 125 independent Myx<sup>r</sup> mutants (Table S3). Sequencing indicates that 106 of the 125 independent Myx<sup>r</sup> mutants are single-substitution mutants. The single-substitution mutants comprise 18 distinct substitutions, involving 2 sites within β' (residue 345 in β' conserved region C and residue 1351 in β' conserved region H) and 11 sites within β (residues 1255, 1275, 1278, 1279, 1285, 1298, 1315, 1317, 1320, 1322, and 1325 in and near β conserved region I; Table S3; Fig. S1B). In the three-dimensional structure of RNAP, the sites of the Myx<sup>r</sup> substitutions define a single determinant with dimensions of ~20 Å × ~20 Å × ~10 Å (Fig. 2B). The determinant is located in the RNAP switch region and encompasses a significant fraction of the RNAP switch region, including switch 2 and segments of β' and β adjacent to switch 2 (Fig. 2B). We conclude that the RNAP switch region contains an extensive determinant for function of Myx.

All identified Myx<sup>r</sup> substitutions involve residues that are conserved in bacterial RNAP (Fig. S2), consistent with the observation that Myx exhibits broad-spectrum activity against bacterial RNAP. Three identified Myx<sup>r</sup> substitutions involve residues that are not conserved--and indeed are radically different--in eukaryotic RNAPI, RNAP II, and RNAP III (β residues 1275, 1279, and 1322; Fig. S2), consistent with observation that Myx does not exhibit activity against eukaryotic RNAP.

**The RNAP switch region contains a binding determinant for Myx**—Equilibrium binding experiments with wild-type RNAP and with a representative Myx<sup>r</sup> RNAP derivative, [Arg345]β'-RNAP, indicate that the Myx<sup>r</sup> RNAP derivative exhibits a dramatically lower affinity for myxopyronin ( $K_d = 0.6 \pm 0.3 \mu\text{M}$  for wild-type RNAP vs.  $K_d > 10 \mu\text{M}$  for [Arg345]β'-RNAP; Fig. 2C). We conclude that the RNAP switch region contains a binding determinant for Myx.

The inferred binding site for Myx is remote from the binding site for rifamycins (Figs. 1A, 2B). Consistent with this, Myx<sup>r</sup> mutants do not exhibit cross-resistance with rifampicin (Table 1), and rifampicin-resistant mutants do not exhibit cross-resistance with Myx (Hu et al., 1998; O'Neill et al., 2000; M. Talaue, N. Connell, J.M., and R.H.E., unpublished).

The inferred binding site for Myx also is remote from the RNAP active center (Fig. 2B) and from binding sites for nucleic acids and nucleotides (Ebright, 2000; Darst, 2001; Cramer, 2002; Young et al., 2002; Murakami and Darst, 2003). Indeed, the inferred binding site for Myx is nearly completely buried within the base of the β' pincer (Fig. 2B). We infer that it is unlikely that Myx functions through direct steric interactions with the active center, nucleic acids, or nucleotides, and infer that it is likely that Myx functions through an allosteric mechanism. Noting that the RNAP switch region serves as the hinge that mediates opening and closing of the RNAP clamp (Fig. 1; Cramer et al., 2001; Gnatt et al., 2001; Cramer, 2002), we suggest that Myx functions by binding to the RNAP switch region and interfering with opening and closing of the RNAP clamp--preventing the clamp from opening to permit DNA to enter the active-center cleft during early stages of transcription initiation, and/or preventing the clamp from closing to retain DNA in the active-center cleft during late stages of transcription initiation and during transcription elongation.

### Biochemical basis of transcription inhibition by Myx

Transcription involves the following reactions (Record et al., 1996; Young et al., 2002; Murakami and Darst, 2003): (i) RNAP binds to promoter DNA, to yield an RNAP-promoter closed complex (RP<sub>c</sub>); (ii) RNAP inserts positions -11 to +15 of the promoter DNA into the RNAP active-center cleft, to yield an RNAP-promoter intermediate complex (RP<sub>i</sub>); (iii) RNAP unwinds positions -11 to +2 of promoter DNA, to yield an RNAP-promoter open complex

(RP<sub>o</sub>); (iv) RNAP enters into initial synthesis of RNA, engaging in cycles of synthesis and release of short RNA products (abortive RNA products), as an RNAP-promoter initial transcribing complex (RP<sub>itc</sub>); and (v), upon synthesis of an RNA product of a critical threshold length of ~9–11 nt, RNAP breaks its interactions with promoter DNA and enters into processive synthesis of RNA as an RNAP-DNA elongation complex (RD<sub>e</sub>).

**Myx inhibits transcription initiation**—As a first step to determine the biochemical basis of transcription inhibition by Myx, we performed run-off transcription experiments (methods as in Mukhopadhyay et al., 2004). The results indicate that Myx inhibits the formation of both abortive RNA products (products of transcription initiation; 3 nt and 4 nt species produced in large stoichiometric excess over the DNA template) and full-length RNA products (products of transcription initiation followed by transcription elongation; species produced in stoichiometric equivalence with the DNA template) (Figs. 3A, S3A). Within experimental error, the median effective concentrations, IC<sub>50</sub>s, for inhibition of formation of abortive products and full-length products are identical to each other ( $1.7 \pm 0.6 \mu\text{M}$  vs.  $1.3 \pm 0.3 \mu\text{M}$ ; Fig. 3A) and are identical to the equilibrium dissociation constant, K<sub>d</sub>, for RNAP-Myx interaction ( $0.6 \pm 0.3 \mu\text{M}$ ; Fig. 2C). The inhibition is specific and requires the RNAP switch region; a Myx<sup>r</sup> substitution in the RNAP switch region abrogates inhibition (Figs. 3A, S3B). The inhibition exhibits a profound order-of-addition-dependence; inhibition is observed only when interaction of RNAP with Myx is allowed to precede interaction of RNAP with promoter DNA (Figs. 3A, S3C). Fluorescence-detected abortive initiation assays confirm that Myx inhibits formation of abortive products, confirm that inhibition is switch-region-dependent, and confirm that inhibition is order-of-addition-dependent (Fig. S4). The observation that Myx inhibits formation of abortive products, indicates that Myx inhibits transcription initiation or inhibits both transcription initiation and transcription elongation. The observation that inhibition requires interaction of RNAP with Myx prior to interaction of RNAP with promoter DNA suggests that Myx inhibits transcription initiation and does not (or at least does not effectively) inhibit transcription elongation.

**Myx inhibits interaction of RNAP with promoter DNA**—To determine whether Myx inhibits steps in transcription initiation up to and including formation of a stable, heparin-resistant RNAP-promoter open complex, we performed fluorescence-detected electrophoretic mobility-shift experiments (methods as in Mukhopadhyay et al., 2004). The results indicate that Myx inhibits formation of a stable, heparin-resistant RNAP-promoter open complex (Figs. 3B, S5). Within experimental error, the IC<sub>50</sub> for the inhibition ( $0.8 \pm 0.3 \mu\text{M}$ ; Fig. 3B, S5) is identical to the IC<sub>50</sub> for inhibition of transcription and the K<sub>d</sub> for RNAP-Myx interaction ( $1.3 \pm 0.3 \mu\text{M}$  and  $0.6 \pm 0.3 \mu\text{M}$ ; Figs. 2C, 3A). The inhibition is specific and requires the RNAP switch region; a Myx<sup>r</sup> substitution in the RNAP switch region abrogates inhibition (Fig. 3B, S5). The inhibition exhibits the same profound order-of-addition-dependence as observed for inhibition of transcription; the inhibition is observed only when interaction of RNAP with Myx is allowed to precede interaction of RNAP with promoter DNA (Fig. 3B, S5). Equivalent results are obtained with all promoters tested, including consensus -35/-10 promoters, non-consensus -35/-10 promoters, and extended -10 promoters (Figs. 3B, S5). We conclude that Myx functions by preventing interaction of RNAP with promoter DNA to form a stable, heparin-resistant RNAP-promoter open complex--preventing either DNA binding, DNA retention, or both. We note that this conclusion is consistent with the proposal above that Myx functions by interfering with opening and/or closing of the RNAP clamp--preventing clamp opening required for DNA binding and/or preventing clamp closing required for DNA retention.

**Myx inhibits interaction of RNAP with promoter positions -11 to +15**—To map the RNAP-promoter interaction inhibited by Myx, we performed fluorescence-detected electrophoretic mobility-shift experiments with promoter subfragments. The results indicate

that inhibition does not occur with promoter subfragments that lack promoter positions  $-11$  to  $+15$  (Figs. 3C, S6). Thus Myx does not inhibit formation of a stable, heparin-resistant complex of RNAP with a DNA fragment that lack positions  $-11$  to  $+15$  of the template strand and positions  $-6$  to  $+15$  of the nontemplate strand (“fork-junction” DNA fragment; Guo and Gralla, 1998; Murakami and Darst, 2002b) (Fig. 3C,S6). Equivalent results are obtained with fork-junction DNA fragments having sequences of other promoters and with fork-junction DNA fragments having different-length nontemplate-strand overhangs (Figs. 3C,S6). We infer Myx interferes with interactions of RNAP with the promoter DNA segment comprising positions  $-11$  to  $+15$ . We note that positions  $-11$  to  $+15$  correspond, precisely, to the positions that are proposed to bind within the RNAP active-center cleft, and to be affected by opening and closing of the RNAP clamp, in structural models of transcription-initiation complexes (Naryshkin et al, 2000; Ebright, 2000; Young et al., 2002; Murakami and Darst, 2003). We suggest that Myx functions by interfering with opening and/or closing of the RNAP clamp—preventing clamp opening required for entry of promoter positions  $-11$  to  $+15$  and/or preventing clamp closing required for retention of promoter positions  $-11$  to  $+15$ .

**Myx inhibits interaction of RNAP with promoter positions  $-11$  to  $+15$  in double-stranded form**—The promoter DNA segment comprising positions  $-11$  to  $+15$  contains the region that is unwound during transcription initiation to form the “transcription bubble” (positions  $-11$  to  $+2$ ; Record et al., 1996; Young et al., 2002; Murakami and Darst, 2003). To determine whether the RNAP-promoter interaction inhibited by Myx involves the transcription-bubble region in double-stranded form, in single-stranded DNA form, or both, we performed fluorescence-detected electrophoretic mobility-shift experiments with promoter derivatives in which the transcription-bubble region was constrained to be in single-stranded form. The results indicate that inhibition does not occur if the transcription-bubble region is constrained to be in single-stranded form (Figs. 3D–F, S7). Thus Myx does not inhibit formation of stable, heparin-resistant complexes of RNAP with DNA fragments in which positions  $-11$  to  $+2$  are maintained in single-stranded form by the presence of noncomplementary template- and nontemplate-strand sequences (“artificial-bubble” DNA fragment; Tripatara and deHaseth, 1993; Helmann and deHaseth, 1999), by the presence of a template-strand gap (“template-strand-gap” DNA fragment), or by the presence of a nontemplate-strand gap (“nontemplate-strand-gap” DNA fragment) (Figs. 3D–F). Myx also does not inhibit formation of stable, heparin-resistant complexes of RNAP with an oligonucleotide comprising positions  $-21$  to  $+15$  of the nontemplate strand (“nontemplate-strand oligonucleotide”; Marr and Roberts, 1997) (Fig. S7). Equivalent results are obtained in experiments using RNAP and DNA concentrations that are one-tenth those in the experiments in Fig. 3 and that are unequivocally sub-saturating, ruling out the possibility that inhibition occurs but is masked by a high affinity of RNAP for DNA fragments in which positions  $-11$  to  $+2$  are in single-stranded form (Fig. S8). Further results indicate that Myx has no effect on equilibrium dissociation constants for RNAP-DNA interaction,  $K_{d,RNAP-DNA}$ , for DNA fragments in which positions  $-11$  to  $+2$  are in single-stranded form (Fig. S9). We infer that Myx interferes with interactions of RNAP with the promoter DNA when—and only when—the transcription-bubble region is in double-stranded form. We note that transcription-bubble region interacts with RNAP in double-stranded form in early stages of transcription initiation, before and during entry of DNA into the RNAP active-center cleft (in  $RP_c$  and  $RP_i$ ), but interacts with RNAP in single-stranded form in late stages of transcription initiation, after entry of DNA into the RNAP active-center cleft (in  $RP_o$  and  $RP_{itc}$ ; Record et al., 1996; Young et al., 2002; Murakami and Darst, 2003). We propose that Myx functions in early stages of transcription initiation, before or during entry of DNA into the RNAP active-center cleft (in  $RP_c$  or  $RP_i$ ). We note further that structures of RNAP suggest that opening of the RNAP clamp is required for entry of double-stranded DNA (diameter  $\sim 20$  Å) into the RNAP active-center cleft, but not for entry of single-stranded DNA (diameter  $\sim 7$  Å) into the RNAP active-center

cleft (see Murakami and Darst, 2002a; Vassilyev et al., 2002). We propose that Myx functions by interfering with opening of the RNAP clamp in early stages of transcription initiation--preventing clamp opening required for entry of promoter positions  $-11$  to  $+15$ , in double-stranded form, into the RNAP active-center cleft in early stages of transcription initiation.

According to this proposal, Myx inhibits formation of stable, heparin-resistant complexes of RNAP with DNA fragments that contain promoter positions  $-11$  to  $+15$  in double-stranded form by preventing clamp opening and blocking entry of double-stranded DNA into the RNAP active-center cleft, thereby blocking establishment of RNAP-DNA interactions essential for heparin-resistance (interactions that minimally involve positions  $-11$  to  $-7$  of one DNA strand; Guo and Gralla, 1998; Helmann and DeHaseth, 1999). According to this proposal, Myx does not inhibit formation of stable, heparin-resistant complexes of RNAP with DNA fragments that contain the corresponding positions in single-stranded form, since prevention of clamp opening does not block entry of single-stranded DNA into the RNAP active-center cleft.

The artificial-bubble DNA fragment of Fig. 3D is able to serve as a template for transcription (Tripatara and deHaseth, 1993; Helmann and deHaseth, 1999). Myx does not efficiently inhibit transcription from the artificial-bubble DNA fragment at concentrations at which it efficiently inhibits transcription from promoter DNA fragments (Fig. S10). A DNA fragment having a 3'-terminal single-stranded overhang also is able to serve as a template for transcription ("tailed template"; Kadesch and Chamberlin, 1982). Myx does not efficiently inhibit transcription from a tailed template at concentrations at which it efficiently inhibits transcription from promoter DNA fragments (Fig. S11). A single-stranded closed-circular DNA construct also is able to serve as a template for transcription ("rolling-circle-transcription template"; Daubendiek and Kool, 1997). Myx does not efficiently inhibit transcription from the rolling-circle-transcription template at concentrations at which it efficiently inhibits transcription from promoter DNA fragments (Fig. S12). We infer that Myx, in the relevant concentration range, does not efficiently inhibit steps in transcription subsequent to interaction of RNAP with promoter positions  $-11$  to  $+15$  in double-stranded form (the step bypassed by use of artificial-bubble, tailed, and rolling-circle-transcription templates).

### Structural basis of transcription inhibition by Myx

We have determined a crystal structure of *Thermus thermophilus* RNAP holoenzyme in complex with Myx. [Myx inhibits *T. thermophilus* RNAP holoenzyme with  $IC_{50} = 20 \mu M$  (J.M. and R.H.E., unpublished).] Crystals of RNAP-Myx were obtained by soaking pre-existing crystals of RNAP in solutions containing Myx, X-ray diffraction data were collected at the Brookhaven National Light Source beamline X-25, and the structure was solved by molecular replacement and refined to a resolution of  $3.0 \text{ \AA}$  (96% complete), an  $R_{work}$  of  $= 0.233$ , and an  $R_{free}$  of  $0.288$  (Table 2; Figs. S13, S14). The structure defines the location of the binding site for Myx, defines contacts between Myx and RNAP, and defines effects of Myx on RNAP conformation.

**Myx interacts with the RNAP switch region**—Myx binds within the RNAP switch region, consistent with the genetic data above (Fig. 4A). Myx makes direct interactions with switch 1 and, especially, switch 2 ( $\beta'$  residues 1319–1328 and 330–347), and also makes direct interactions with adjacent segments of the  $\beta'$  and  $\beta$  subunits ( $\beta'$  residues 1346–1357 and  $\beta$  residues 1270–1292 and 1318–1328) (Fig. 4B). [Here and elsewhere in the text, to facilitate comparison of structural data to genetic and biochemical data obtained with *E. coli* RNAP, residues are numbered as in *E. coli* RNAP. In the figures, residues are numbered, in parallel, as in *T. thermophilus* RNAP and as in *E. coli* RNAP.] The interactions with switch 1 and switch 2 involve residues conserved both in bacterial RNAP and in eukaryotic RNAP I, RNAP II, and RNAP III; the interactions with adjacent segments of  $\beta'$  and  $\beta$  involve residues conserved in

bacterial RNAP but not conserved in eukaryotic RNAP I, RNAP II, or RNAP III, consistent with the selectivity of Myx. Myx contacts, or is within 5 Å of, all residues at which substitutions conferring high-level ( $\geq 16$ -fold) Myx-resistance are obtained (Fig. 4B).

Myx does not overlap the RNAP active-center cleft or the predicted positions of nucleic acids in transcription initiation and elongation complexes (Fig. 4A). Indeed, Myx is nearly completely buried, with little surface accessibility on the interior of the RNAP active-center cleft and with no surface accessibility on the exterior of RNAP. These observations support the inference from genetic data above that Myx must inhibit transcription through allosteric interactions, not through direct, steric interactions.

**Myx interacts with a nearly completely enclosed, primarily hydrophobic, binding pocket in the RNAP switch region**—Myx interacts with a nearly completely enclosed, primarily hydrophobic, binding pocket (Fig. 5). The binding pocket is crescent-shaped, has dimensions of  $\sim 25$  Å (measured along the curve of the crescent)  $\times \sim 5$  Å  $\times \sim 4$  Å, and has a volume of  $\sim 500$  Å<sup>3</sup> (Fig. 5A, C). The binding pocket connects to an adjacent hydrophobic pocket having a volume of  $\sim 120$  Å<sup>3</sup> (Fig. 5A, C). The adjacent hydrophobic pocket is located close to the terminus of the Myx dienone sidechain, and, as such, potentially is able to accommodate the one-carbon sidechain extension present in myxopyronin B (see Irschik et al., 1983; Kohl et al., 1983) and the seven-carbon sidechain extension present in Cor (see Irschik et al., 1985; Jansen et al., 1985; see section on Cor, below). The divider between the binding pocket and the adjacent hydrophobic pocket is formed by the sidechain of  $\beta$ Leu1326 (see section on Cor, below). The binding pocket connects to the RNAP active-center cleft through an opening with dimensions of  $\sim 5$  Å  $\times \sim 4$  Å (Fig. 5A, C). The opening is located close to the C16–C17 methyl and the C15 carbonyl of the Myx dienone sidechain and to the C4 hydroxyl of the Myx  $\alpha$ -pyrone ring. We propose that Myx accesses the binding pocket by entering the RNAP active-center cleft and threading through this opening.

Contacts between residues of RNAP and Myx are shown in Fig. 5B and are summarized in Fig. 5C. A network of H-bonds centered on an ordered bound water molecule engages the nitrogen atom and both oxygen atoms of the enecarbamate moiety of Myx. The network involves the ordered bound water molecule (which yields unequivocal electron density; Fig. S14), the sidechain ammonium of  $\beta'$  Lys1348, the sidechain carboxyl of  $\beta'$  Asp802, and the sidechain indole NH of  $\beta$ Trp1276. The sidechain carboxyl of  $\beta$ Glu1279 forms an H-bond with the carbonyl oxygen of the enecarbamate moiety of Myx; formation of this H-bond is expected to require either protonation of the carboxyl of  $\beta$ Glu1279 or tautomerization of the enecarbamate of Myx. The sidechain hydroxyl of  $\beta$ Ser1322 potentially forms an H-bond with the C2 carbonyl oxygen of the  $\alpha$ -pyrone ring of Myx. The backbone NH of  $\beta'$  Gly620 potentially forms an H-bond with the C4 hydroxyl of the  $\alpha$ -pyrone ring of Myx. Residues 801, 805, and 1348 of  $\beta'$  and residues 1034, 1038, 1041, 1271, 1275, 1279, and 1291 of  $\beta$  make van der Waals interactions with the enecarbamate sidechain of Myx. Residues 344, 345, 346, and 1352 of  $\beta'$  and residue 1322 of  $\beta$  make van der Waals interactions with the  $\alpha$ -pyrone ring of Myx; side-chain methylene groups of  $\beta'$ Lys345 underlie, and essentially form a platform for, the  $\alpha$ -pyrone ring of Myx. Residues 339, 1323, 1324, 1328, and 1352 of  $\beta'$  and residue 1326 of  $\beta$  make extensive van der Waals interactions with the dienone sidechain of Myx.

Four substitutions conferring high-level ( $\geq 16$ -fold) resistance to Myx are predicted to disrupt RNAP-Myx H-bonds ( $\beta$ 1279Glu $\rightarrow$ Gly,  $\beta$ 1279Glu $\rightarrow$ Lys,  $\beta$ Ser1322 $\rightarrow$ Pro, and  $\beta$ Ser1322 $\rightarrow$ Val), and at least one of these is predicted also to introduce steric conflict with Myx ( $\beta$ 1279Glu $\rightarrow$ Lys). Five substitutions conferring high-level resistance to Myx are predicted to disrupt favorable RNAP-Myx van der Waals interactions and to introduce steric clash with Myx ( $\beta'$ 345Lys $\rightarrow$ Arg,  $\beta'$ 345Lys $\rightarrow$ Asn,  $\beta'$ 345Lys $\rightarrow$ Thr,  $\beta$ 1275 Val $\rightarrow$ Met, and

$\beta$ 1279Val $\rightarrow$ Phe). The remaining substitution conferring high-level resistance to Myx is predicted to introduce steric conflict with Myx ( $\beta$ '1351Val $\rightarrow$ Phe).

With one exception, the structure is consistent with, and can account for, published structure-activity relationships for synthetic Myx analogs (Doundoulakis et al., 2004; Lira et al., 2007). The one exception involves O-methylation of the C4 hydroxyl of the  $\alpha$ -pyrone ring of Myx--which the structure predicts would disrupt an intramolecular H-bond important for establishing the orientation of the dienone sidechain relative to the  $\alpha$ -pyrone ring, would disrupt a potential intermolecular H-bond, and would introduce steric clash (Fig. 5B, C and text above), but which the published work indicates does not have large effects on RNAP-Myx interaction (Lira et al., 2007). Re-synthesis and re-testing of the O-methyl analog indicates that the published work is incorrect, and that O-methylation in fact profoundly impairs RNAP-Myx interaction (A. Wasmuth, Y. Sun, C. Self, G. Olson, J.M., and R.H.E., unpublished).

The structure suggests opportunities for preparation of optimized Myx analogs, including: (i) appending functionality at C24, potentially enabling formation of interactions with residues at and in the adjacent hydrophobic pocket; (ii) appending functionality at C17, potentially enabling formation of interactions with residues at and in the RNAP active-center-cleft; (iii) replacing the enecarbamate carbonyl oxygen by an H-bond donor, potentially enabling formation of an H-bond with  $\beta$ Glu1041 without the requirement for (presumably unfavorable) tautomerization of the enecarbamate or (presumably unfavorable) protonation of  $\beta$ Glu1041; and (iv) appending a hydroxyl or analogous group at the position of the enecarbamate nitrogen, potentially enabling formation of an H-bond network with  $\beta$ 'Lys1463,  $\beta$ 'Asp802, and  $\beta$ Trp1276 without the requirement for (presumably unfavorable) recruitment and immobilization of a water molecule.

**Myx interacts with an RNAP conformational state in which the RNAP clamp and RNAP switch region are in a partly closed, or partly closed to fully closed, conformation**—The RNAP clamp in the crystal structure of RNAP-Myx adopts the same clamp conformation as in the crystal structure of unliganded RNAP in the same crystal form: i.e., a partly closed clamp conformation (Figs. 4A, S13A–B; see Vassylyev et al. 2002). This observation permits the conclusion that binding of Myx is compatible with a partly closed clamp conformation. However, this observation does not permit the conclusion that binding of Myx favors, stabilizes, or induces an intermediate clamp conformation, since clamp conformation in this crystal form is constrained by, and may be determined by, crystal-lattice interactions (crystal-lattice interactions with the clamp, with a  $\beta$ ' non-conserved domain appended to the clamp, and with a  $\sigma$  domain associated with the clamp).

The RNAP switch-region in the crystal structure of RNAP-Myx adopts a different conformation from that in the crystal structure of unliganded RNAP in the same crystal form (Fig. S15). The difference in conformation involves a nine-residue segment of switch 2—a nine-residue segment that differs in conformation in open, partly closed, and fully closed clamp conformational states ( $\beta$ ' residues 336–344; Fig. 1B). The difference in conformation involves 1–4 Å displacements of C $\alpha$  atoms of the nine-residue segment toward positions intermediate between those in partly closed and fully closed clamp conformational states (Figs. S15,1B). The nine-residue segment contains a residue that contacts template-strand DNA in transcription complexes ( $\beta$ ' residue 339; see Gnatt et al., 2001; Vassylyev et al., 2007); however, since Myx does not efficiently inhibit interaction between RNAP and template-strand DNA in relevant concentration ranges (Figs. 3D, F, S10–S12), possible differences in interaction between the nine-residue segment and template-strand DNA cannot, in of themselves, account for transcription inhibition by Myx.

### Target and mechanism of transcription inhibition by Cor

Cor is a polyketide-derived  $\alpha$ -pyrone antibiotic structurally related to Myx (Fig. 1C; Irschik et al., 1985; Jansen et al., 1985). Cor is produced by the myxobacterium *Corallocooccus coralloides* Cc c127 (Irschik et al., 1985; Jansen et al., 1985). The compound inhibits growth of a broad spectrum of Gram-positive and Gram-negative bacterial species, including *M. tuberculosis*, *S. aureus*, *S. pneumoniae*, *B. anthracis*, and *E. coli* DH21tolC (MICs  $\leq 12.5$   $\mu\text{g/ml}$  for all; MIC  $\leq 0.1$   $\mu\text{g/ml}$  for *S. aureus*; Irschik et al., 1985; M. Talaue, N. Connell, J.M. and R.H.E., unpublished). The compound is bacteriocidal, as assessed in experiments with *E. coli* DH21f2tolC (J.M. and R.H.E., unpublished). The compound inhibits bacterial RNAP (IC<sub>50</sub>  $\sim 4$   $\mu\text{M}$ ) but does not inhibit eukaryotic RNAP II (Irschik et al., 1985).

Cor differs from Myx only by possession of a seven-carbon extension of the dienone sidechain (Fig. 1C).

Perhaps unsurprisingly, in view of the structural similarity between Myx and Cor, analysis of cross-resistance patterns indicates that all mutants that exhibit high-level ( $\geq 16$ -fold) resistance to Myx also exhibit resistance to Cor (Table 1). We infer that Cor interacts with a target that overlaps the target for Myx. To define further the target for Cor, we performed saturation mutagenesis--targeting codons for RNAP residues located within 30 Å of sites of Myx-resistant, Cor-cross-resistant mutants--and we isolated and characterized more than 75 additional Cor-resistant mutants (Table S4; Fig. S16). With one exception, all identified substitutions that confer high-level ( $\geq 8$ -fold) resistance to Cor also confer resistance to Myx (Table 1). We conclude that Cor interacts with the same target as Myx.

The one exception--a substitution that confers high-level resistance to Cor but that does not confer resistance to Myx--involves  $\beta$ residue 1326 ( $\beta 1326\text{Leu}\rightarrow\text{Trp}$ ; Table 1). We infer that  $\beta$  residue 1326 interacts with the seven-carbon sidechain extension present in Cor but not in Myx. Consistent with this inference, in the three-dimensional structure of the RNAP-Myx complex,  $\beta 1326$  is located close to the ligand dienone sidechain terminus, the point of attachment of the seven-carbon sidechain extension present in Cor (Fig. 5A–C). Further consistent with this inference, in the three-dimensional structure of the RNAP-Myx complex,  $\beta 1326$  forms one wall of an adjacent hydrophobic pocket that would have sufficient volume to accommodate the seven-carbon sidechain extension present in Cor if  $\beta 1326$  is Leu (as in the wild-type enzyme) but not if  $\beta 1326$  is Trp (as in the mutant enzyme) (Fig. 5A, C).

Experiments addressing the biochemical basis of transcription inhibition by Cor indicate that Cor inhibits transcription initiation, prevents interaction of RNAP with promoter DNA, prevents interaction with promoter positions  $-11$  to  $+15$ , and prevents interaction with promoter positions  $-11$  to  $+15$  when, and only when, these positions are in double-stranded form (Figs. S17, S18). We conclude that Cor shares the same target and same mechanism as Myx.

### Target and mechanism of transcription inhibition by Rip

Rip is a polyketide-derived macrocyclic-lactone antibiotic structurally unrelated to Myx and Cor (Fig. 1C; Irschik et al., 1995; Augustiniak et al., 1996). Rip is produced by the myxobacterium *Sorangium cellulosum* So ce377 (Irschik et al., 1995; Augustiniak et al., 1996). The compound inhibits growth of *S. aureus*, and *E. coli* DH21tolC (MICs  $\leq 1$   $\mu\text{g/ml}$ ; Irschik et al., 1995; J.M. and R.H.E., unpublished). The compound is bacteriocidal, as assessed in experiments with *E. coli* DH21f2tolC (J.M. and R.H.E., unpublished). The compound inhibits bacterial RNAP (IC<sub>50</sub>  $\sim 0.8$   $\mu\text{M}$ ) but does not inhibit eukaryotic RNAP II (Irschik et al., 1995).

Rip exhibits no structural similarity to Myx and Cor, apart from a general similarity in size and hydrophobic character (Fig. 1C).

Surprisingly, in view of the lack of structural similarity, analysis of cross-resistance patterns indicates that all identified mutants that exhibit high-level resistance to Myx and Cor also exhibit resistance to Rip (Table 1). We infer that Rip interacts with a target that overlaps the target for Myx and Cor. To define further the target for Rip, we performed saturation mutagenesis--targeting codons for RNAP residues located within 30 Å of sites of Myx-resistant, Rip-cross-resistant mutants--and we isolated and characterized 50 additional Rip-resistant mutants (Table S5; Fig. S19). With one exception ( $\beta$ 1326Leu→Trp; see preceding section), all identified substitutions conferring high-level resistance to Rip also confer resistance to Myx (Table 1). Without exception, all identified substitutions conferring high-level resistance to Rip also confer resistance to Cor (Table 1). We conclude that Rip interacts with the same target as Myx and Cor.

Experiments addressing the biochemical basis of transcription inhibition by Rip indicate that Rip inhibits transcription initiation, prevents interaction of RNAP with promoter DNA, prevents interaction with promoter positions -11 to +15, and prevents interaction with promoter positions -11 to +15 when, and only when, these positions are in double-stranded form (Figs. S20, S21). We conclude that Rip, despite its lack of structural similarity to Myx and Cor, shares the same target and mechanism as Myx and Cor. We conclude, thus, that at least two different chemotypes, the  $\alpha$ -pyrone chemotype and the macrocyclic-lactone chemotype, function through this target and mechanism.

## Discussion

Our genetic results establish that Myx interacts with the RNAP switch region (Figs. 2, S1, S2)--i.e., with the hinge that mediates rotation of the RNAP clamp relative to the remainder of RNAP and, thus, that mediates opening and closing of the RNAP active-center cleft (Fig. 1A, B). Our biochemical results establish that Myx inhibits interactions of RNAP with promoter DNA, establish that Myx inhibits interactions with the promoter DNA segment that enters the RNAP active-center cleft during transcription initiation (i.e., promoter positions -11 to +15), and establish that Myx inhibits interactions with this promoter DNA segment when it is in a double-stranded state (i.e., the state present before and during entry of promoter DNA into the RNAP active-center cleft, during early stages of transcription initiation) but not when it is present in a single-stranded state (i.e., the state present after entry of promoter DNA into the RNAP active-center cleft, during late stages of transcription initiation) (Figs. 3; S3–S12). Our structural results define contacts between Myx and RNAP and indicate that Myx interacts with an RNAP conformational state in which the RNAP clamp and RNAP switch region are in a partly closed, or partly closed to fully closed, conformation (Figs. 4, 5, S13–S15). Based on these results, we propose that Myx inhibits transcription by locking the RNAP switch region in one conformation and thereby locking the RNAP clamp in one conformation--a partly closed, or partly closed to fully closed, conformation--thereby preventing opening of the RNAP active-center cleft to permit entry of double-stranded DNA during transcription initiation. According to this proposal, Myx functions essentially by “hinge jamming.”

Our results further indicate that two other antibiotics--the structurally related  $\alpha$ -pyrone antibiotic Cor and the structurally unrelated macrocyclic-lactone antibiotic Rip--share the same target as Myx and the same mechanism as Myx (Table 1; Figs. S16–S21).

The results define a new target and a new mechanism for inhibition of RNAP. The results, further, provide experimental evidence for functional significance of the RNAP switch region, experimental evidence for functional significance of opening and closing of the RNAP clamp,

and experimental evidence supporting the hypothesis that the RNAP clamp must open to permit DNA to enter the RNAP active-center cleft during transcription initiation. As such, the results have implications for understanding mechanisms of transcription and mechanisms of transcriptional regulation.

Based on several considerations, we suggest that the RNAP switch region is an exceptionally attractive target for discovery of new broad-spectrum antibacterial therapeutic agents. First, the switch region comprises residues that are highly conserved in both Gram-positive bacterial RNAP and Gram-negative bacterial RNAP (Fig. S2)--providing a basis for broad-spectrum activity of compounds that function through the switch region. Second, the switch region contains residues that are not conserved, and indeed are radically different, in human RNAP I, RNAP II, and RNAP III (Fig. S2)--providing a basis for therapeutic selectivity of compounds that function through the switch region. Third, the switch region is distant from the binding site for rifamycins (Fig. 1A) and from the binding sites for other characterized inhibitors of bacterial RNAP (see Darst et al., 2004; Chopra, 2007), providing a basis for absence of cross-resistance with rifamycins (Table 1) and for absence of cross-resistance with other characterized inhibitors of bacterial RNAP (unpublished). Fourth, the ligand binding site in the switch region comprises a nearly completely enclosed, predominantly hydrophobic, pocket (Fig. 5A, C), providing a basis for efficient “druggability” by multiple chemotypes (Table 1; Figs. 1C, 2, S16, S19), facilitating *in silico* rational design of optimized ligands, and facilitating *in silico* virtual screening for new ligands.

We point out that the mechanistic role of the RNAP switch region (hinge for movement of domains) and the structural character of the ligand binding site in the RNAP switch region (nearly completely enclosed, predominantly hydrophobic, pocket) are reminiscent of the mechanistic role and structural character of the HIV-1 reverse transcriptase NNRTI site (non-nucleoside reverse-transcriptase inhibitor site; Kohlstaedt et al., 1992; Tantillo et al., 1994; Sluis-Cremer et al., 2004). The HIV-1 reverse transcriptase NNRTI site is druggable by multiple chemotypes and is the target for multiple antiviral agents in current clinical use. We suggest that the RNAP switch region may exhibit similarly high druggability and similarly high utility.

Priorities for basic research include determination of structures of complexes of RNAP with Cor and Rip (to define interactions with the seven-carbon-atom sidechain extension in Cor and to define interactions with the macrocyclic-lactone chemotype of Rip) and determination of effects of switch-region-target inhibitors on RNAP clamp conformation and dynamics in solution (addressable by use of fluorescence resonance energy transfer; A. Chakraborty, Y. Korlann, D. Wang, S. Weiss, and R.H.E., unpublished). Priorities for applied research include cloning and surrogate-host expression of biosynthetic genes for Myx, Cor, and Rip (to overcome an important obstacle to possible clinical application of Myx, Cor, and Rip--namely, the relatively poor fermentation characteristics of the myxobacterial strains that produce these compounds), *in silico* rational design of optimized switch-region-target inhibitors, and *in silico* virtual screening and *in vitro* target-directed high-throughput screening for new switch-region-target inhibitors.

## Experimental Procedures

Full details of Experimental Procedures are presented in the Supplement.

## Mutagenesis

Random mutagenesis was performed by use of PCR amplification, exploiting the baseline error rate of PCR amplification (methods analogous to those in Mukhopadhyay et al., 2004, but with PCR amplification of entire plasmid molecules using Pfu DNA polymerase). Saturation

mutagenesis was performed by use of PCR amplification with “doped” primers (methods analogous to those in Mukhopadhyay et al. 2004, but using pooled sets of “doped” primers).

### Microbiological assays

Complementation assays and MIC assays were performed essentially as in Tuske et al., 2005.

### RNAP-Myx interaction assays

RNAP-Myx interaction was detected by monitoring quenching by Myx of fluorescence emission of RNAP Trp residues ( $\lambda_{\text{ex}} = 280 \text{ nm}$ ;  $\lambda_{\text{em}} = 330 \text{ nm}$ ).

### RNAP-DNA interaction assays

RNAP-DNA interaction assays were performed essentially as in Mukhopadhyay et al., 2004.

### Transcription assays

Run-off transcription assays and fluorescence-detected abortive initiation assays were performed essentially as in Mukhopadhyay et al., 2004. Rolling-circle transcription assays were performed using the Kool NC-45 kit (Epicentre, Inc.).

### Structure determination

Crystallization, crystal handling, data collection, structure solution, and refinement were performed by methods analogous to those in Tuske et al., 2005. Atomic coordinates and structure factors for RNAP-Myx have been deposited in the PDB (PDB accession number 3DXJ).

### Supplementary Material

Refer to Web version on PubMed Central for supplementary material.

### Acknowledgements

We thank A. Chakraborty, N. Connell, S. Darst, Y. Korlann, C. Self, Y. Sun, G. Olson, M. Talaue, D. Wang, X. Wang, A. Wasmuth, and S. Weiss for unpublished data and G. Höfle, M. Kalesse, and E. Sineva for discussion. This work was supported by NIH grant AI072766 to R.H.E. and E.A., NIH grant GM41376 to R.H.E., and a Howard Hughes Medical Investigatorship to R.H.E.

### References

- Augustiniak H, Irschik H, Reichenbach H, Höfle G. Ripostatin A, B, and C: isolation and structure elucidation of novel metabolites from *Sorangium cellulosum*. *Liebigs Ann Chem* 1996;10:1657–1663.
- Campbell E, Korzheva N, Mustaev A, Murakami K, Nair S, Goldfarb A, Darst S. Structural mechanism for rifampicin inhibition of bacterial RNA polymerase. *Cell* 2001;104:901–912. [PubMed: 11290327]
- Chopra I. Bacterial RNA polymerase: a promising target for the discovery of new antimicrobial agents. *Curr Opin Investig Drugs* 2007;8:600–607.
- Cramer P. Multisubunit RNA polymerases. *Curr Opin Struct Biol* 2002;12:89–97. [PubMed: 11839495]
- Cramer P, Bushnell D, Fu J, Gnat A, Maier-Davis B, Thompson N, Burgess R, Edwards A, David P, Kornberg R. Architecture of RNA polymerase II and implications for the transcription mechanism. *Science* 2000;288:640–649. [PubMed: 10784442]
- Cramer P, Bushnell D, Kornberg R. Structural basis of transcription: RNA polymerase II at 2.8 angstrom resolution. *Science* 2001;292:1863–1876. [PubMed: 11313498]
- Darst S. Bacterial RNA polymerase. *Curr Opin Struct Biol* 2001;11:155–162.

- Darst S. New inhibitors targeting bacterial RNA polymerase. *Trends Biochem Sci* 2004;29:159–162. [PubMed: 15124627]
- Daubendiek S, Kool E. Generation of catalytic RNAs by rolling transcription of synthetic DNA nanocircles. *Nature Biotech* 1997;15:273–277.
- Doundoulakis T, Xiang A, Lira R, Agrios K, Webber S, Sisson W, Aust R, Shah A, Showalter R, Appleman J, Simonsen K. Myxopyronin B analogs as inhibitors of RNA polymerase, synthesis and biological evaluation. *Bioorg Med Chem Lett* 2004;14:5667–5672. [PubMed: 15482944]
- Ebright R. RNA polymerase: structural similarities between bacterial RNA polymerase and eukaryotic RNA polymerase II. *J Mol Biol* 2000;304:687–698. [PubMed: 11124018]
- Gnatt A, Cramer P, Fu J, Bushnell D, Kornberg R. Structural basis of transcription: an RNA polymerase II elongation complex at 3.3 Å resolution. *Science* 2001;292:1876–1882. [PubMed: 11313499]
- Guo Y, Gralla J. Promoter opening via a DNA fork junction binding activity. *Proc Natl Acad Sci USA* 1998;95:11655–11660. [PubMed: 9751721]
- Helmann JD, deHaseth P. Protein-nucleic acid interactions during open complex formation investigated by systematic alteration of the protein and DNA binding partners. *Biochem* 1999;38:5959–5967. [PubMed: 10320321]
- Hu T, Schaus J, Lam K, Palfreyman M, Wuonola M, Gustafson G, Panek J. Total synthesis and preliminary antibacterial evaluation of the RNA polymerase inhibitors (+/-)-Myxopyronin A and B. *J Org Chem* 1998;63:2401–2406.
- Irschik H, Gerth K, Höfle G, Kohl W, Reichenbach H. The myxopyronins, new inhibitors of bacterial RNA synthesis from *Myxococcus fulvus* (*Myxobacteriales*). *J Antibiot* 1983;36:1651–1658. [PubMed: 6420386]
- Irschik H, Jansen R, Höfle G, Gerth K, Reichenbach H. The coralopyronins, new inhibitors of bacterial RNA synthesis from *Myxobacteria*. *J Antibiot* 1985;38:145–152. [PubMed: 2581926]
- Irschik H, Augustiniak H, Gerth K, Höfle G, Reichenbach H. The ripostatins, novel inhibitors of eubacterial RNA polymerase isolated from myxobacteria. *J Antibiot* 1995;48:787–792. [PubMed: 7592022]
- Jansen R, Irschik H, Reichenbach H, Höfle G. Coralopyronin A, B, and C: three novel antibiotics from *Coralococcus coralloides* Cc c127 (*Myxobacteriales*). *Liebigs Ann Chem* 1985;4:822–836.
- Kadesch T, Chamberlin M. Studies of in vitro transcription by calf thymus RNA polymerase II using a novel duplex DNA template. *J Biol Chem* 1982;257:5286–5295. [PubMed: 7068686]
- Kohl W, Irschik H, Reichenbach H, Höfle G. Antibiotics from gliding bacteria. XVII. Myxopyronin A and B: two novel antibiotics from *Myxococcus fulvus* strain Mx f50. *Liebigs Ann Chem* 1983;1983:1656–1667.
- Kohlstaedt L, Wang J, Friedman J, Rice P, Steitz T. Crystal structure at 3.5 Å resolution of HIV-1 reverse transcriptase complexed with an inhibitor. *Science* 1992;256:1783–1790. [PubMed: 1377403]
- Lira R, Xiang A, Doundoulakis T, Biller W, Agrios K, Simonsen K, Webber S, Sisson W, Aust R, Shah A, et al. Syntheses of novel myxopyronin B analogs as potential inhibitors of bacterial RNA polymerase. *Bioorg Med Chem Lett* 2007;17:6797–6800. [PubMed: 17980587]
- Marr M, Roberts J. Promoter recognition as measured by binding of polymerase to nontemplate strand oligonucleotide. *Science* 1997;276:1258–60. [PubMed: 9157885]
- Mukhopadhyay J, Sineva E, Knight J, Levy R, Ebright R. Antibacterial peptide microcin J25 inhibits transcription by binding within, and obstructing, the RNA polymerase secondary channel. *Mol Cell* 2004;14:739–751. [PubMed: 15200952]
- Murakami K, Darst S. Bacterial RNA polymerases. *Curr Opin Structl Biol* 2003;13:31–39.
- Murakami K, Masuda S, Darst S. Structural basis of transcription initiation: RNA polymerase holoenzyme at 4 Å resolution. *Science* 2002a;296:1280–1284. [PubMed: 12016306]
- Murakami K, Masuda S, Campbell E, Muzzin O, Darst S. Structural basis of transcription initiation: an RNA polymerase holoenzyme-DNA complex. *Science* 2002b;296:1285–1290. [PubMed: 12016307]
- Naryshkin N, Revyakin A, Kim Y, Mekler V, Ebright R. Structural organization of the RNA polymerase-promoter open complex. *Cell* 2000;101:601–611. [PubMed: 10892647]

- Record, MT.; Reznikoff, W.; Craig, M.; McQuade, K.; Schlax, P. *Escherichia coli* RNA polymerase ( $E\sigma^{70}$ ), promoters, and the kinetics of the steps of transcription initiation. In: Neidhardt, F., editor. *Escherichia coli* and *Salmonella*. Washington, D.C.: ASM Press; 1996. p. 792-820.
- Sluis-Cremer N, Temiz N, Bahar I. Conformational changes in HIV-1 reverse transcriptase induced by nonnucleoside reverse transcriptase inhibitor binding. *Curr HIV Res* 2004;2:323–332. [PubMed: 15544453]
- Tantillo C, Ding J, Jacobo-Molina A, Nanni R, Boyer P, Hughes S, Pauwels R, Andries K, Janssen P, Arnold E. Locations of anti-AIDS drug binding sites and resistance mutations in the three-dimensional structure of HIV-1 reverse transcriptase. Implications for mechanisms of drug inhibition and resistance. *J Mol Biol* 1994;243:369–387. [PubMed: 7525966]
- Tripatara A, deHaseth P. A new start site for *Escherichia coli* RNA polymerase at an engineered short region of non-complementarity in double-stranded DNA. *J Mol Biol* 1993;233:349–358. [PubMed: 8411149]
- Tuske S, Sarafianos S, Wang X, Hudson B, Sineva E, Mukhopadhyay J, Birktoft J, Leroy O, Ismail S, Clark A, et al. Inhibition of bacterial RNA polymerase by streptolydigin: stabilization of a straight-bridge-helix active-center conformation. *Cell* 2005;122:541–552. [PubMed: 16122422]
- Vassilyev D, Sekine S, Laptenko O, Lee J, Vassilyeva M, Borukhov S, Yokoyama S. Crystal structure of a bacterial RNA polymerase holoenzyme at 2.6 Å resolution. *Nature* 2002;417:712–719. [PubMed: 12000971]
- Vassilyev D, Vassilyeva M, Perederina A, Tahirov T, Artsimovitch I. Structural basis for transcription elongation by bacterial RNA polymerase. *Nature* 2007;448:157–162. [PubMed: 17581590]
- Young B, Gruber T, Gross C. Views of transcription initiation. *Cell* 2002;109:417–420. [PubMed: 12086598]
- Zhang G, Campbell E, Minakhin L, Richter C, Severinov K, Darst S. Crystal structure of *Thermus aquaticus* core RNA polymerase at 3.3 Å resolution. *Cell* 1999;98:811–824. [PubMed: 10499798]

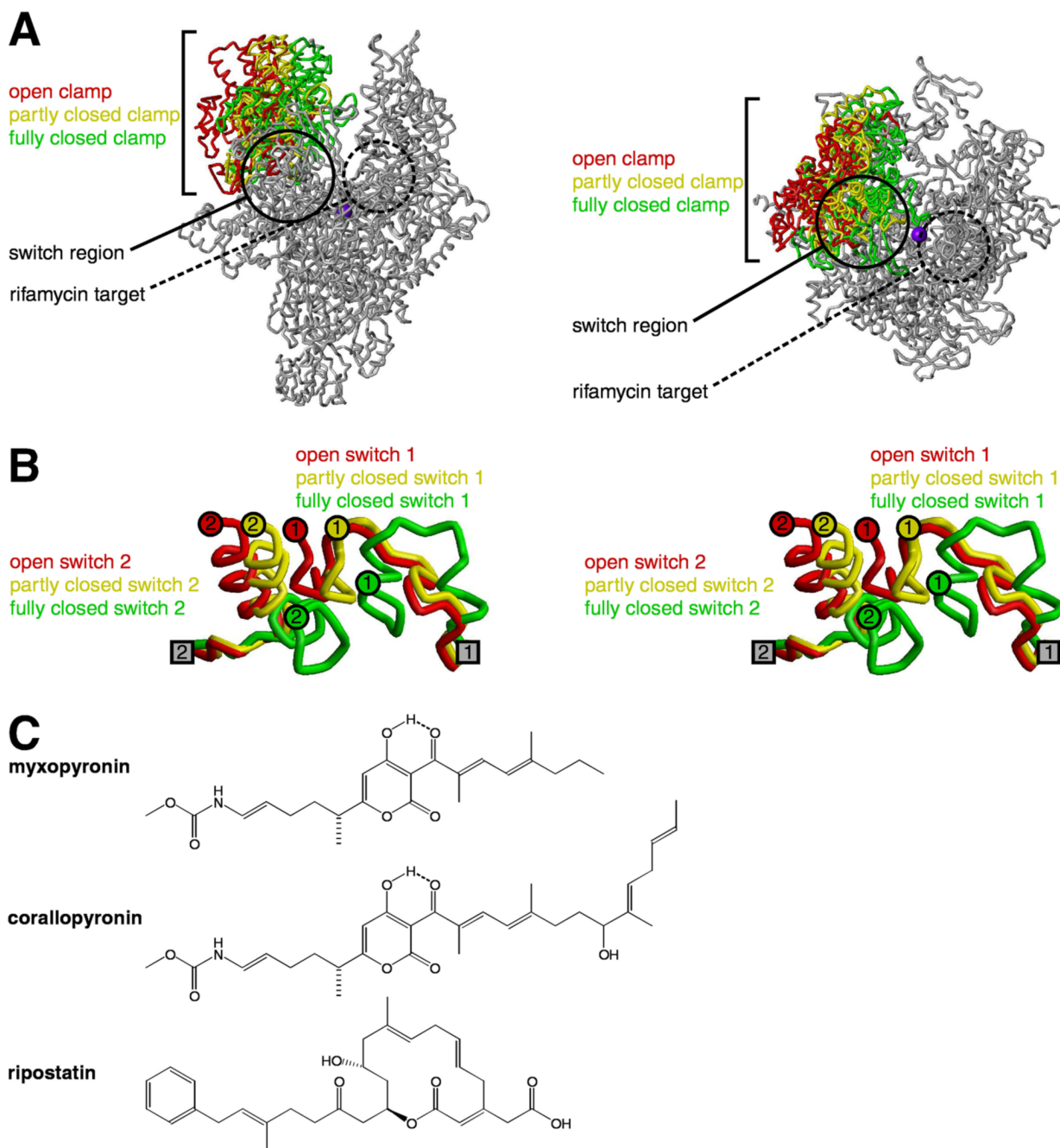


**Fig. 1. RNAP clamp, RNAP switch region, and antibiotics studied**

(A) Conformational states of the RNAP clamp (two orthogonal views). Structure of RNAP showing open (red), partly closed (yellow), and fully closed (green) clamp conformations, as observed in crystal structures (PDB 1I3Q, PDB 1HQM, PDB 1I6H). Circle, switch region; dashed circle, binding site for rifamycins; violet sphere, active-center  $Mg^{2+}$ .

(B) Conformational states of the RNAP switch region (stereoview). Structure of RNAP switch 1 and RNAP switch 2 ( $\beta'$  residues 1304–1329 and  $\beta'$  residues 330–349; residues numbered as in *E. coli* RNAP) showing conformational states associated with open (red), partly closed (yellow), and fully closed (green) clamp conformations, as observed in crystal structures (PDB 1I3Q, PDB 1HQM, PDB 1I6H). Gray squares, points of connection of switch 1 and switch 2

to the RNAP main mass. Colored circles, points of connection of switch 1 and switch 2 to the RNAP clamp.

(C) Structures of myxopyronin A (Myx), coralopyronin A (Cor), and ripostatin A (Rip).

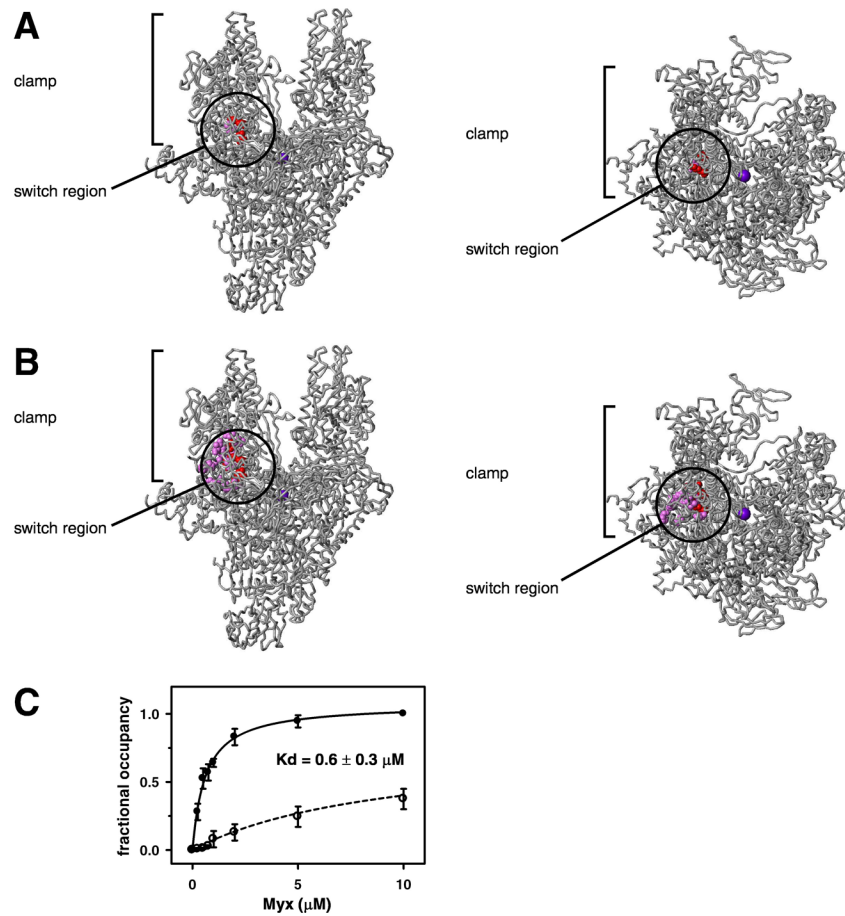


**Fig. 2. Target of transcription inhibition by Myx**

(A)–(B) Structure of RNAP showing sites of single-residue substitutions that confer resistance to Myx (high-level resistance in red; moderate-level resistance in pink; Tables S1, S3) (two orthogonal views). Substitutions from random mutagenesis are in (A). Substitutions from random and saturation mutagenesis are in (B). Atomic coordinates are for *T. thermophilus* RNAP holoenzyme (PDB 2CW0;  $\sigma$  subunit and  $\beta'$ -subunit non-conserved region omitted for clarity). View orientations are as in Fig. 1A. Violet sphere, active-center  $\text{Mg}^{2+}$ . (C) Results of fluorescence-quenching experiments assessing binding of Myx to wild-type RNAP (filled circles) and to Myx<sup>r</sup> RNAP ([Arg345] $\beta'$ -RNAP; open circles). Means  $\pm$  3SE.

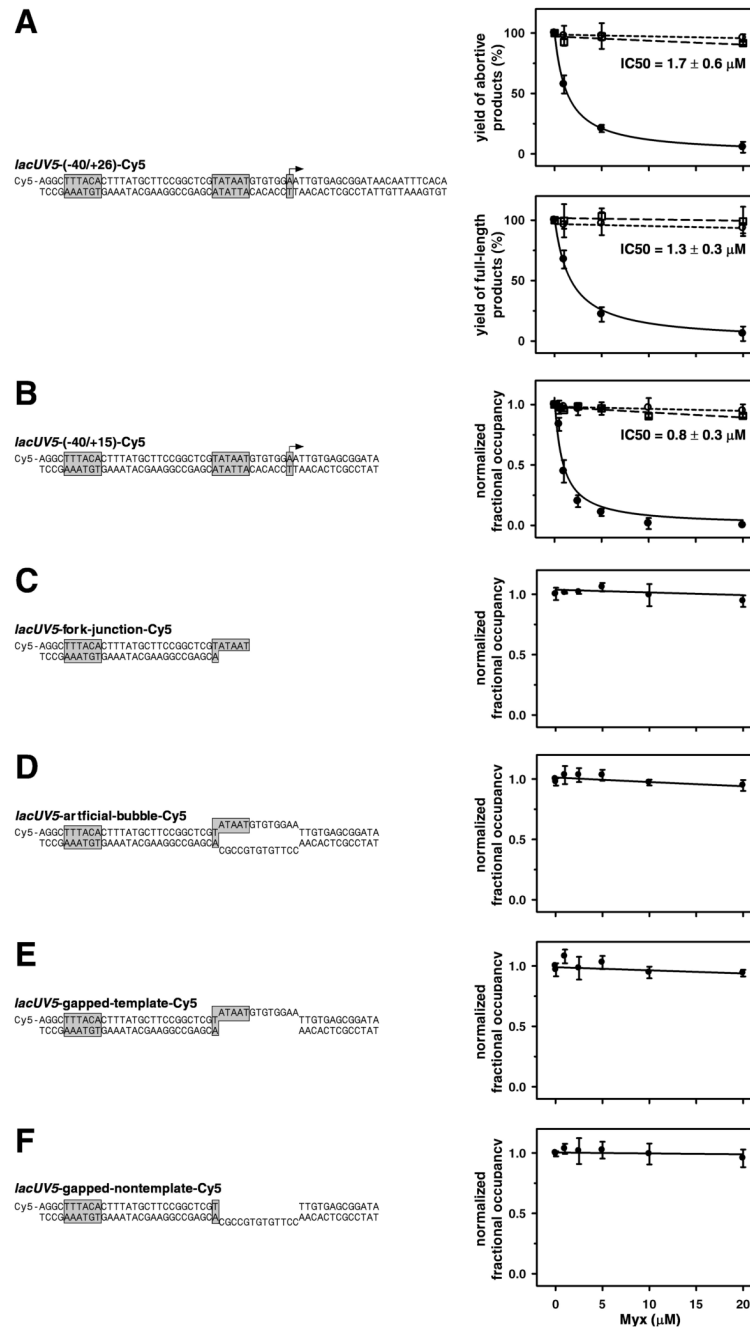


**Fig. 3. Biochemical basis of transcription inhibition by Myx**

(A) Results of run-off transcription experiments assessing effects of Myx on formation of abortive products (top right) and full-length products (bottom right). Left panel, promoter DNA fragment. Right panels, data from experiments with wild-type RNAP (filled circles), Myx<sup>r</sup> RNAP ([Arg345]β'-RNAP; open circles), and wild-type RNAP with Myx added after addition of DNA (open squares). Means ± 3SE.

(B) Results of fluorescence-detected electrophoretic mobility-shift experiments assessing effects of Myx on interaction of RNAP with promoter DNA. Left panel, promoter DNA fragment. Right panels, data for experiments with wild-type RNAP (filled circles), Myx<sup>r</sup> RNAP

([Arg345] $\beta'$ -RNAP; open circles), and wild-type RNAP with Myx added after addition of DNA (open squares). Means  $\pm$  3SE.

**(C)–(F)** Results of fluorescence-detected electrophoretic mobility-shift experiments assessing effects of Myx on interaction of RNAP with fork-junction (C), artificial-bubble (D), gapped-template-strand (E), and gapped-template-strand (F) DNA fragments. Left panels, DNA fragments. Right panels, data.

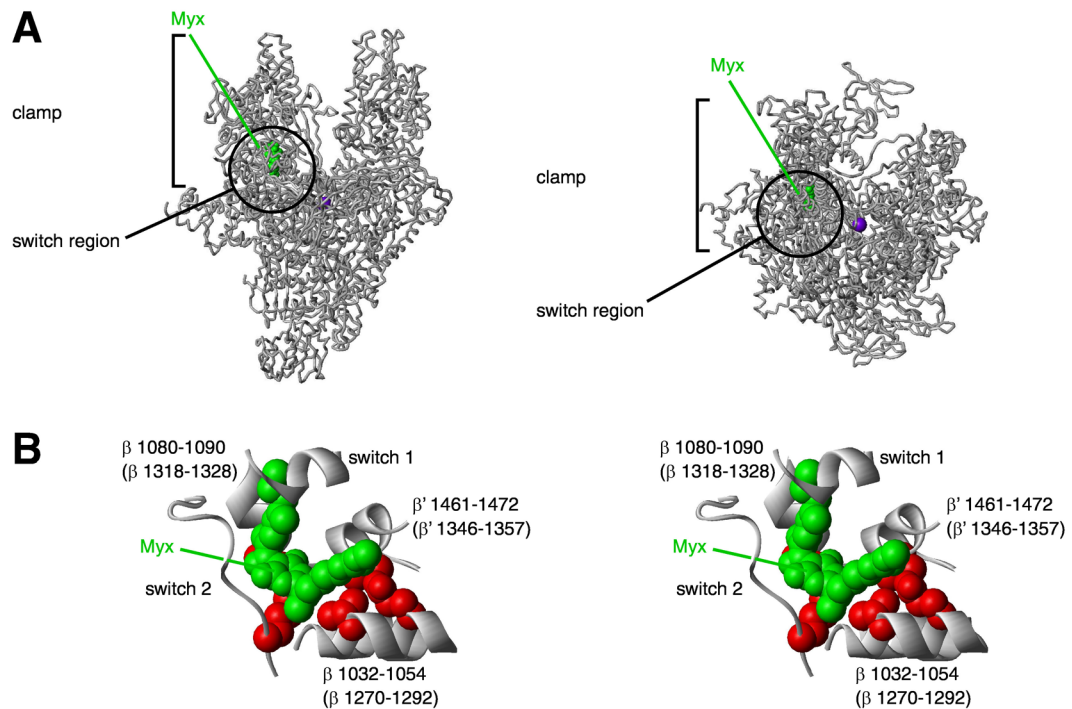


**Fig. 4. Structural basis of transcription inhibition by Myx: structure of the RNAP-Myx complex**  
 (A) Overall structure (two orthogonal views;  $\beta'$  non-conserved region and  $\sigma$  omitted for clarity). View orientations are as in Fig. 1A. Green, Myx; violet sphere, active-center  $Mg^{2+}$ .  
 (B) Myx binding region (stereoview). Residues are numbered both as in *T. thermophilus* RNAP and as in *E. coli* RNAP (in parentheses). Green, Myx; red, sites of single-residue substitutions that confer high-level resistance to Myx.

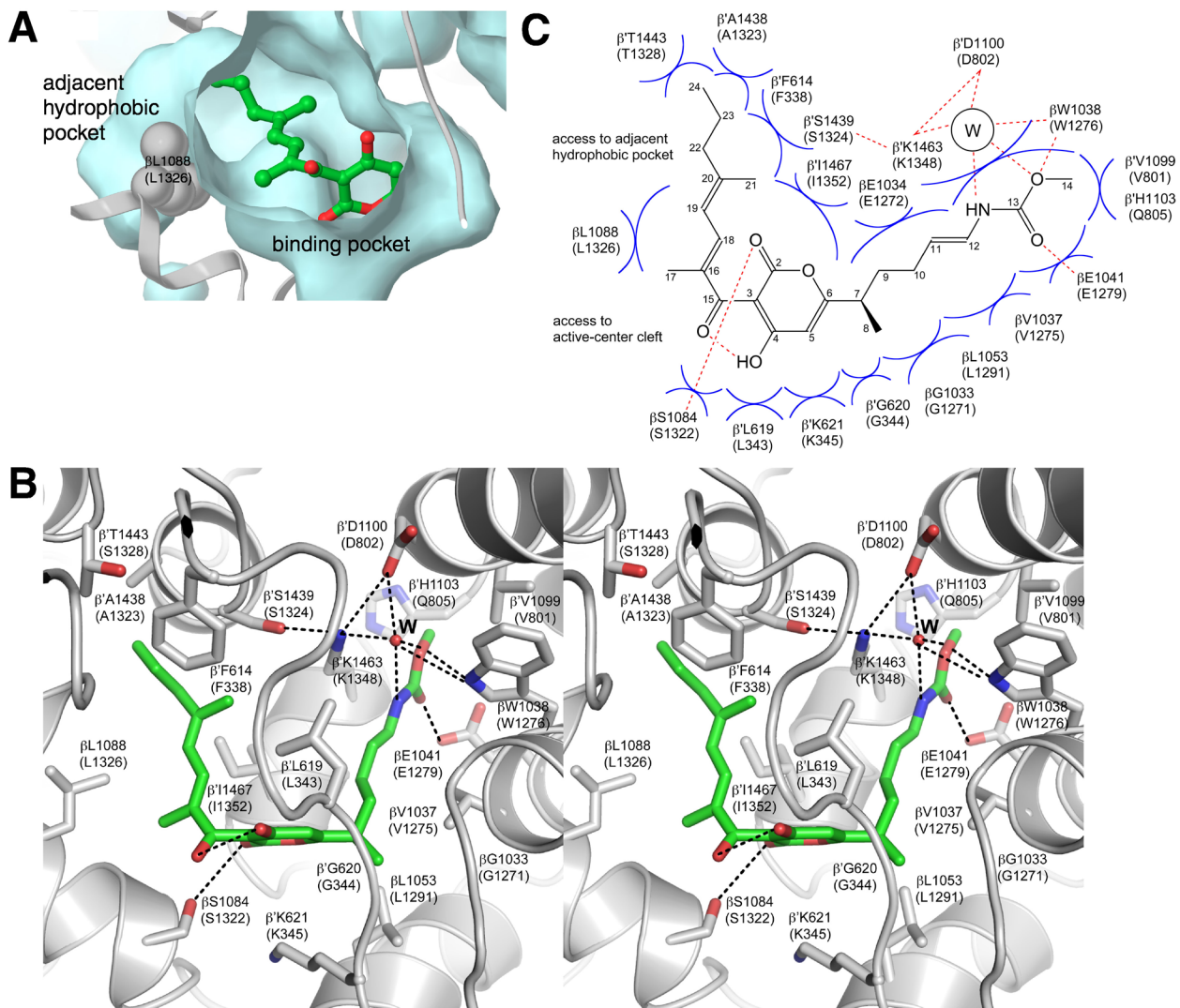


**Fig. 5. Structural basis of transcription inhibition by Myx: contacts between RNAP and Myx**  
 (A) Binding pocket for Myx (view through opening that provides access to the RNAP active-center cleft). Cyan, surface representation of the binding pocket and the adjacent hydrophobic pocket. Gray, ribbon representation of RNAP backbone. Green, Myx carbon atoms; red, Myx oxygen atoms. RNAP residues are numbered both as in *T. thermophilus* RNAP and as in *E. coli* RNAP (in parentheses).

(B) Contacts between RNAP and Myx (stereoview). Gray, RNAP backbone (ribbon representation) and RNAP sidechain carbon atoms (stick representation); green, Myx carbon atoms; red, oxygen atoms; blue, nitrogen atoms. “W,” ordered bound water molecule. Dashed lines, H-bonds.

(C) Schematic summary of contacts between RNAP and Myx. “W,” ordered bound water molecule. Red dashed lines, H-bonds. Blue arcs, van der Waals interactions.

Table 1

## Myx/Cor/Rip cross-resistance patterns

amino acid substitution	selected resistance(s)			
	Myx	Cor	Rip	Rif
<b>RNAP β' subunit</b>				
345 Lys→Arg	>32	>8	>16	1
345 Lys→Asn	32	8	8	1
345 Lys→Thr	32	8	>16	1
1346 Gly→Asp	1	4	4	1
1351 Val→Phe	>32	>8	>16	1
1352 Ile→Asn	2	4	>16	1
1352 Ile→Ser	2	4	>16	1
1354 Gly→Cys	2	2	4	1
<b>RNAP β subunit</b>				
1232 Met→Ile	2	4	4	1
1255 Thr→Ile	2	4	4	1
1275 Val→Met	>32	>8	8	1
1275 Val→Phe	>32	>8	>16	1
1278 Leu→Val	2	4	>16	1
1279 Glu→Gly	32	4	>16	1
1279 Glu→Lys	>32	8	4	1
1283 Ala→Val	2	4	4	1
1285 Tyr→Asp	2	1	4	1
1291 Leu→Phe	2	1	4	1
1298 Val→Leu	2	2	4	1
1315 Met→Leu	2	2	4	1
1317 Pro→Leu	2	2	2	1
1320 Pro→Ala	2	4	4	1
1322 Ser→Pro	32	4	>16	1
1322 Ser→Thr	2	4	4	1
1322 Ser→Tyr	2	4	2	1
1322 Ser→Val	16	8	>16	1
1325 Val→Leu	2	4	4	1
1326 Leu→Trp	1	>8	>16	1

<sup>a</sup>MIC values with wild-type RNAP β' and wild-type RNAP β for Myx, Cor, Rip, and Rif are 0.1, 1.6, 0.1, and 0.1 µg/ml, respectively.

**Table 2**Crystallographic data and refinement statistics<sup>a,b</sup>

crystallographic data	
beamline	BNL-NLSL X25
space group	P6 <sub>5</sub>
temperature (°C)	-165
wavelength (Å)	1.1
resolution range (Å)	50.0–3.0
cell parameters: a, b, c (Å)	235.09, 235.09, 250.88
completeness (%) (highest shell, 3.11–3.00 Å)	96.0 (77.4)
reflections (total/unique)	556, 296/150, 817
R <sub>merge</sub>	0.11 (0.71)
refinement statistics	
space group	P3 <sub>2</sub>
resolution range (Å)	50.0–3.0
number of reflections (R <sub>free</sub> set)	298, 910 (2,351)
cutoff criteria	F  < 0
R <sub>work</sub>	0.233
R <sub>free</sub>	0.288
number of refined atoms	56, 128
bond-length rmsd (Å)	0.008
bond-angle rmsd (°)	1.56

$$^a R_{\text{merge}} = \frac{\sum_{hkl} \sum_i |I(hkl)_i - \langle I(hkl) \rangle|}{\sum_{hkl} \sum_i \langle I(hkl)_i \rangle}$$

<sup>b</sup>  $R_{\text{work}} = \frac{\sum_{hkl} |F_{\text{O}}(hkl) - F_{\text{C}}(hkl)|}{\sum_{hkl} |F_{\text{O}}(hkl)|}$ , where  $F_{\text{O}}$  and  $F_{\text{C}}$  are observed and calculated structure factors, respectively. The crystals have the symmetry of space group P3<sub>2</sub> with perfect (50%) hemihedral twinning and twinning operator (–h, –k, l), leading to apparent hexagonal (P6/m) intensity symmetry. Processing and scaling were carried out in P6<sub>5</sub> followed by expansion to P3<sub>2</sub> for structure solution and refinement